Spectroscopic and Magnetostructural Correlations in Oxo-Bridged Dinuclear Vanadium(III) Complexes of Potential Biological Significance

Marcus R. Bond,[‡,§] Roman S. Czernuszewicz,*[,†] Bakul C. Dave,[†,||] Qing Yan,[†] Madan Mohan,[‡] Ruben Verastegue,[‡] and Carl J. Carrano*[,‡]

Departments of Chemistry, University of Houston, Houston, Texas 77204, and Southwest Texas State University, San Marcos, Texas 78666

Received June 28, 1995[⊗]

The synthesis of several dinuclear (μ-oxo)bis(μ-carboxylato or diphenylphosphato) divanadium(III) complexes, $[V_2O(O_2CR)_2L_2]$ (where L = $HB(pz)_3^-$ and R = CH_3 (**I**), C_6H_5 (**II**), C_2H_5 (**III**), and H (**IV**), or L = $HB(3,5\text{-}Me_2pz)_3^-$ and R = CH_3 (**V**)) and $[V_2O(O_2P(OC_6H_5)_2)_2(HB(pz)_3)_2]$ (**X**), are described. X-ray crystallographic analysis of **III** and **X** gave the following parameters: **III**, $C_{32}H_{42}B_2N_{16}O_5V_2$, $P2_1/n$, a = 13.406(3) Å, b = 15.313(3) Å, c = 22.217(4) Å, β = 106.75(3)°, Z = 4, V = 4367(2) Å^3; **X**, $C_{44}H_{43}B_2N_{13}O_9P_2V_2$, $P2_1/n$, a = 11.944(4) Å, b = 20.091(7) Å, c = 21.729(16) Å, β = 94.38(4)°, Z = 4, V = 5199(4) Å^3. Protonation of the oxo-bridged species with either $HClO_4$ or HSO_3CF_3 causes a rapid color change from deep green to pale red and results in the crystallization of the hydroxo-bridged species $[V_2(OH)(O_2CR)_2(HB(pz)_3)_2](X)$ (where R = CH_3 and X = ClO_4^- (**VI**) or R = C_2H_5 (**VII**), C_6H_5 (**VIII**), and H (**IX**), and X = $CF_3SO_3^-$) and $[V_2(OH)(O_2P(OC_6H_5)_2)_2(HB(pz)_3)_2](CF_3SO_3)$ (**XI**). Crystallographic parameters are as follows: **VIIb**, $C_{29}H_{39}B_2F_3N_{12}O_9SV_2$, $P2_12_12_1$, a = 12.309(3) Å, b = 16.197(2) Å, c = 20.232(2) Å, Z = 4, V = 4033.9(9) Å^3; **XI**, $C_{56.5}H_{64.5}B_2F_3N_{12}O_{14.5}P_2SV_2$, $P\bar{1}$, a = 12.113(2) Å, b = 14.938(3) Å, c = 20.052(4) Å, α = 72.88(3)°, β = 76.73(3)°, γ = 87.15(3)°, Z = 4, V = 3374.3(11) Å^3. In contrast to well-studied oxo-bridged Fe(III) complexes, UV–visible, paramagnetic NMR, resonance Raman, and magnetic susceptibility on these V(III) complexes reveal electronic and magnetostructural correlations dependent on the V–O–V angle. Such correlations may be useful in assigning structures to complex biosystems containing the $[V(\mu\text{-}O)V]^{4+}$ core.

Introduction

Oxo-bridged dinuclear transition metal complexes occupy an important place in modern inorganic chemistry. Study of these species derives from interests in magnetic exchange, electron transfer interactions, catalysis, and modeling of metalloproteins. The Fe(III)[1] and Mn(III)[2] systems have been studied extensively while those of the early transition metals, V(III) in particular, have received attention only recently.[3] Nevertheless, two basic structural motifs have been described and studied for oxo-bridged V(III) dimers: one type contains an unsupported and linear (or nearly so) oxo bridge and the other type a supported (μ-oxo)bis(μ-carboxylato) core in which the oxo bridge is bent.[4]

Our interest in these systems stems in part from the fact that oxo-bridged vanadium(III) dimers have also been implicated in the biochemistry of tunicates. Certain species of tunicates have long been known to concentrate vanadium, primarily as V(III), in their blood cells.[5,6] Upon cell lysis ascidian blood rapidly turns bright red, a characteristic first recognized by Henze.[7] Although there is no structural data available on the chromophore in "Henze's solution", model compound studies and UV–visible spectroscopic measurements carried out in solution are all consistent with the formation of an oxo-bridged divanadium(III) core.[8–10] While X-ray crystallography provides the most definitive and precise structural information on large biomolecules, its application is frequently beset with the difficulties of growing single crystals. In contrast, complementary spectroscopic probes of structure do not suffer as much from this limitation and are readily applicable to aqueous solutions, the ubiquitous biological medium. Hence one of the main goals of our research program is to provide spectro- and magnetostructural relationships for oxo-bridged vanadium dimers. By establishing relationships between the structures of small well-defined molecules, as determined by X-ray crystallography, and spectral and magnetic properties, such as UV–visible and resonance Raman spectroscopies as well as magnetic exchange coupling constants, it may be possible to extract detailed structural data from complex biosystems such as tunicate blood.

* Authors to whom correspondence should be addressed.
† University of Houston.
‡ Southwest Texas State University.
§ Present address: Department of Chemistry, Southeast Missouri State University, Cape Girardeau, MO 63701.
|| Present address: Department of Chemistry and Biochemistry, University of California at Los Angeles, Los Angeles, CA 90024.
⊗ Abstract published in *Advance ACS Abstracts,* October 15, 1995.

(1) (a) Lippard, S. J. *Chem. Br.* **1986**, *22*, 222. (b) Lippard, S. J. *Angew. Chem., Int. Ed. Engl.* **1988**, *27*, 344. (c) Que, L., Jr.; Scarrow, R. C. *ACS Symp. Ser.* **1988**, *372*, 152. (d) Lippard, S. J. *Chem. Br.* **1986**, *22*, 222. (e) Kurtz, D. M., Jr. *Chem. Rev.* **1990**, *90*, 585. (f) Vincent, J. B.; Oliver-Lilley, G. L.; Averill, B. A. *Chem. Rev.* **1990**, *90*, 1447.
(2) (a) Pecoraro, V. *Photochem. Photobiol.* **1988**, *48*, 249. (b) Brudvig, G. W.; Crabtree, R. H. *Prog. Inorg. Chem.* **1989**, *37*, 99. (c) Vincent, J. B.; Christou, G. *Adv. Inorg. Chem.* **1989**, *33*, 197. (d) Wieghardt, K. *Angew. Chem., Int. Ed. Engl.* **1989**, *28*, 1153. (e) Que, L., Jr.; True, A. E. *Prog. Inorg. Chem.* **1990**, *38*, 98. (f) Thorp, H. H.; Brudvig, G. W. *New. J. Chem.* **1991**, *15*, 479. (g) *Bioinorganic Chemistry of Manganese;* Pecoraro, V. L., Ed.; VCH: New York, 1992.
(3) (a) Rehder, D. *Angew. Chem., Int. Ed. Engl.* **1990**, *30*, 148. (b) Butler, A.; Carrano, C. J. *Coord. Chem. Rev.* **1991**, *109*, 61.
(4) West, B. O., *Polyhedron* **1989**, *8*, 219.
(5) Boeri, E.; Ehrenberg, A. *Arch. Biochem. Biophys.* **1954**, *50*, 404.
(6) Anderson, D. H.; Swinehardt, J. H. *Comp. Biochem. Physiol.* **1991**, *99A*, 585.
(7) Henze, M. *Hoppe-Seyler's Z. Physiol. Chem.* **1911**, *72*, 215.
(8) (a) Kanamori, K.; Ookubo, Y.; Iho, K.; Kaai, K.; Michiba, H. *Inorg. Chem.* **1991**, *30*, 3832. (b) Kanamori, K.; Teraoka, M.; Maeda, K. M.; Okamoto, K.-I. *Chem. Lett.* **1993**, 1731.
(9) Kanamori, K.; Ino, K.; Maeda, K. M.; Fukagawa, M.; Kumada, J.; Eguchi, T.; Okamoto, K.-I. *Inorg. Chem.* **1994**, *33*, 5547.
(10) Kime-Hunt, E.; Spartalian, K.; Holmes, S.; Mohan, M.; Carrano, C. J. *J. Inorg. Biochem.* **1991**, *41*, 125.

0020-1669/95/1334-5857$09.00/0

Recent interest in oxo-bridged V(III) dimers has also been spurred by the discovery of their unusual magnetic properties. Wieghardt and co-workers have reported on the magnetic exchange interactions in a series of homo/heteronuclear (μ-oxo or hydroxo)bis(μ-carboxylato) dimetallic complexes employing the 1,4,7-trimethyl-1,4,7-triazacyclononane capping ligand (Me_3-tacn).[11,12] Most members of this series show weak to strong antiferromagnetic coupling for both the oxo- and hydroxo-bridged forms. The divanadium complexes, however, show strong ferromagnetic exchange interactions in the oxo-bridged species which switch to antiferromagnetic upon protonation of the oxo-bridge. Wieghardt *et al.* were unable to unequivocally establish the structural changes that accompany this switch in sign of the magnetic coupling. By employing the topologically similar hydridotris(pyrazolyl)borate ligand we have been able to characterize magnetically, crystallographically, and spectroscopically both the oxo-bridged complexes and their protonated analogs.[13]

Experimental Section

Materials. All synthetic reactions were carried out under an atmosphere of pure dry argon or nitrogen by utilizing standard Schlenk techniques. Subsequent work-up was carried out in air unless otherwise noted. Solvents were dried and distilled under a blanket of inert gas. DMF and acetonitrile were Burdick and Jackson "distilled in glass" grade and used as received. They were stored under an argon or nitrogen atmosphere after opening. Potassium hydridotris(3,5-dimethyl) and unsubstituted (pyrazolyl)borates were synthesized and purified according to the reported methods.[14] The authenticity of the compounds was checked by mp (bp), IR and proton NMR spectroscopies. Vanadium salts were reagent grade and used as received.

Preparation of Compounds. A. $[V_2O(O_2CCH_3)_2(HB(pz)_3)_2]$ (I). To a stirred solution of 2 g of VCl_3 (0.0127 mol) in DMF was added an equimolar quantity (3.2 g) of $K[HB(pz)_3]$. Upon addition, the mixture turned deep purple and was refluxed for 2 h to assure complete reaction. To the hot solution was added a saturated, degassed solution of sodium acetate in water. After several seconds of stirring, a deep-green precipitate appeared. After cooling, the resulting solid was filtered off and recrystallized from hot acetonitrile. Yield: 44%. Anal. Calcd for $C_{22}H_{26}B_2N_{12}O_5V_2$: C, 39.91; H, 3.96; N, 25.39. Found: C, 39.59; H; 3.84; N, 24.71. The corresponding benzoate, **II**, propionate, **III**, and formate, **IV**, bridged complexes were prepared by analogous procedures using the sodium salt of the appropriate acid.

The hydridotris(3,5-dimethylpyrazolyl)borate (μ-oxo)bis(μ-acetato)-divanadium(III) complex, **V**, was prepared using $HB(3,5\text{-}Me_2pz)_3^-$ as the ligand in place of $HB(pz)_3^-$. It is, however, far less stable than the corresponding unsubstituted complex and was handled under inert atmosphere conditions at all times.

B. $[V_2(OH)(O_2CCH_3)_2(HB(pz)_3)_2](CF_3SO_3)$ (VI). To a solution of **I** in acetonitrile was added an excess of triflic acid (perchloric acid can also be used) dissolved in acetonitrile. The deep-green solution turned a pale pink and was evaporated to dryness. The residue was recrystallized from either acetonitrile or an acetonitrile/THF mixture to give a nearly quantitative yield of the protonated product, **VI**. The corresponding triflate salts of the (μ-hydroxo)bis(carboxylato)divanadium(III) complexes bridged by propionate, **VII**, benzoate, **VIII**, and formate **IX**, were prepared in a like manner. Anal. Calcd for $C_{23}H_{27}B_2N_{12}O_8V_2SF_3 \cdot CH_3CN$: C, 35.20; H, 3.52; N; 21.34. Found: C, 35.54; H, 3.33; N, 21.42. Note: the crystal used for X-ray determination of the diacetate **VI** was the perchlorate salt. **Caution!** *Metal perchlorates are potentially explosive.*

C. $[V_2O(O_2P(OC_6H_5)_2)_2(HB(pz)_3)_2]$ (X). To 1.0 g (1.51 mmol) of **I** in dichloromethane was added 0.76 g (3.02 mmol) of sodium diphenyl phosphate. The resulting deep-green solution was stirred for 1 h and then extracted with H_2O. The green organic layer was dried over sodium sulfate and evaporated to dryness, and the solid residue was recrystallized from acetonitrile. Anal. Calcd for $C_{44}H_{43}N_{13}P_2O_9V_2B$: C, 48.66; H, 3.96; N, 16.77. Found: C, 48.63; H, 4.03; N, 16.77.

D. $[V_2(OH)(O_2P(OC_6H_5)_2)_2(HB(pz)_3)_2](CF_3SO_3)$ (XI). Compound **X** was dissolved in acetonitrile and treated with an excess of triflic acid. The initially deep-green solution turned red. Evaporation of the solvent and recrystallization of the residue from THF/toluene yielded large red crystals of the THF/toluene solvate of **XI** as the triflate salt. Anal. Calcd for $[C_{42}H_{41}N_{12}P_2O_9V_2B_2]CF_3SO_3 \cdot C_4H_8O \cdot 0.5(C_6H_5CH_3)$: C, 46.77; H, 4.04; N, 12.71. Found: C, 46.46; H, 4.07; N, 12.68.

Spectroscopic Measurements. Routine infrared spectra were obtained on a Perkin-Elmer 1600 FT-IR from solid samples in KBr pellets. UV−visible spectra (CH_3CN solution) were recorded on either a Perkin-Elmer 553 or HP 8520 diode array spectrophotometer. Paramagnetic NMR spectra were obtained in either $CDCl_3$ or CD_3CN solution on an IBM-Bruker NR-80 80 MHz FT-NMR spectrometer. The resonance Raman (RR) spectra were obtained by utilizing discrete lines from Coherent K-2 Kr^+ (406.7−676.4 nm), Coherent 90-6 Ar^+ (457.9−514.5 nm), and Liconix 2040 He-Cd (442.1 nm) ion lasers. Typical laser powers employed were 100−200 mW. The scattered radiation was dispersed by a Spex 1403 double monochromator equipped with 1800 grooves/mm holographic gratings and detected by a cooled Hamamatsu 928 photomultiplier tube.[15] The data were collected digitally with a Spex DM3000 microcomputer system at 0.5-cm^{-1} increments and 1-s integration time per data point. Multiple scans (2−4) were averaged to improve signal to noise ratio. All RR spectra were measured with the sample dispersed in KCl pellets, which were either rotated at room temperature in a solid state spinning Raman cell[16] or attached to a cold finger of a liquid N_2 cryostat[17] to avoid thermal decomposition and improve spectral resolution. ^{18}O exchange at the bridging position in **I** and **X** was accomplished by stirring for 1 h the mixture of the respective natural abundance dimer (20 mg) and $H_2{}^{18}O$ (50 μL, 98% ^{18}O, Isotec, Miamisburg, OH) in a small volume of CH_3CN (1 mL). The solvent was then removed in vacuo and the resulting solids were used without further purification. Their Raman spectra showed essentially 100% ^{18}O substitution at the μ-oxo position for **I** and ~60% for **X**. The relative intensity of the ν_s(VOV) band as a function of excitation wavelength for **I** was measured against the 985-cm^{-1} band of the internal standard, K_2SO_4, which was mixed homogeneously with the sample in a spinning KCl pellet.

Electrochemical and Magnetic Susceptibility Measurements. Electrochemical measurements were performed as previously described.[18] Routine room temperature solid state susceptibilities were measured using a Johnson Mathey MSB-1 susceptibility balance. Solution susceptibility data were obtained at room temperature via the Evans method.[19] The samples used for variable temperature magnetic susceptibility measurements were finely ground, then packed and sealed in a gelatin capsule sample holder. Magnetic moment data were measured in the temperature range, 5−270 K, on an LDJ 9600 vibrating sample magnetometer using a previously described procedure.[20] Diamagnetic corrections were calculated using Pascal's constants (**VIIb**) or by empirically fitting a plot of χ vs $1/T$ (**III**, **XI**).

X-ray Crystallography. Dark green crystals of **III** and red crystals of **VIIb** were grown by slow cooling to −20 °C of CH_3CN or CH_3CN/THF solutions, respectively, of the desired complexes after layering with hexane or ether. Following microscopic examination in air in each case, a suitable crystal was sealed in a Lindemann glass capillary and mounted on a Siemens P4 X-ray diffractometer at room temper-

(11) Knopp, P.; Wieghardt, K. *Inorg. Chem.* **1991**, *30*, 4061.
(12) Hotzelmann, R.; Wieghardt, K.; Florke, V.; Haupt, H. J.; Weatherburn, D. C.; Bonvoushin, J.; Blondin, G.; Girerd, J. -J. *J. Am. Chem. Soc.* **1992**, *114*, 1681.
(13) A preliminary account of this work has already appeared. Carrano, C. J.; Verastegue, R.; Bond, M. R. *Inorg. Chem.* **1993**, *32*, 3589.
(14) (a) Trofimenko, S. *J. Am. Chem. Soc.* **1967**, *89*, 6288. (b) Trofimenko, S., *Inorg. Synth.* **1970**, *12*, 99.
(15) Czernuszewicz, R. S. In *Methods in Molecular Biology*; Jones, C.; Mulloy, B.; Thomas, A. H., Eds.; Humana Press: Totowa, NJ, 1993; Vol. 17, pp 345−374.
(16) Czernuszewicz, R. S. *Appl. Spectrosc.* **1986**, *40*, 571.
(17) Czernuszewicz, R. S.; Johnson, M. K. *Appl. Spectrosc.* **1983**, *37*, 297.
(18) Bonadies, J. A., Carrano, C. J. *J. Am. Chem. Soc.* **1986**, *108*, 4088.
(19) Evans, D. F. *J. Chem. Soc.* **1959**, 2003.
(20) Mohan, M.; Bond, M. R.; Otieno, T.; Carrano, C. J. *Inorg. Chem.* **1995**, *34*, 1233.

Table 1. Summary of Crystallographic Data and Data Collection Parameters for **III**, **VIIb**, **X**, and **XI**[a]

	III	VIIb	X	XI
formula	$V_2O_5C_{32}H_{42}N_{16}B_2$	$V_2O_9C_{29}H_{39}N_{12}B_2SF_3$	$V_2O_9C_{44}H_{43}N_{13}B_2P_2$	$V_2O_{14.5}C_{56.5}H_{64.5}N_{12}B_2P_2SF_3$
mol wt	854.3	912.3	1083.4	1418.2
space group	$P2_1/n$	$P2_12_12_1$	$P2_1/n$	$P\bar{1}$
a, Å	13.406(3)	12.309(3)	11.944(4)	12.113(2)
b, Å	15.313(3)	16.197(2)	20.091(7)	14.938(3)
c, Å	22.217(4)	20.232(2)	21.729(16)	20.052(4)
α, deg	90	90	90	72.88(3)
β, deg	106.75(3)	90	94.38(4)	76.73(3)
γ, deg	90	90	90	87.15(3)
V, Å^3	4367(2)	4033.9(9)	5199(4)	3374.3(11)
Z	4	4	4	4
cryst dimns, mm	0.1 × 0.5 × 0.5	0.3 × 0.3 × 0.4	0.2 × 0.2 × 0.3	0.2 × 0.3 × 0.6
cryst dens, g/cm^3	1.299	1.502	1.384	1.396
abs coeff, cm^{-1}	4.84	5.93	4.86	4.34
2θ limits, deg	3.5−45	3.5−43	3.5−45	3.5−45
no. unique data	5575	3133	6733	8553
no. observed data	3595	2333	1006 ($>5\sigma(F)$)	3383
data to param ratio	7.0:1	4.5:1	4.0:1	4.2:1
transmission	0.8328/0.9505	0.8555/0.9422	0.5110/0.8220	0.7765/0.9219
R, R_w[b]	0.0682, 0.0822	0.0499, 0.0509	0.0869, 0.0896	0.0837, 0.1002
max diff peak, e$^-$/Å^3	0.49	0.32	0.54	0.61
Δ/σ, max	0.011	0.000	0.000	0.009

[a] Radiation, graphite-monochromated Mo Kα, $\lambda = 0.71073$ Å; temperature, 298 K. [b] $R = \sum||F_o| - |F_c||/\sum|F_o|$; $R_w = [\sum w(|F_o| - |F_c|)^2/\sum w|F_o|^2]^{1/2}$.

ature. Unit cell parameters were ultimately determined by least-squares refinement of at least 16 well-centered reflections in the range $20 < 2\theta < 30°$. Structure solution (direct methods) and full-matrix least-squares refinement were achieved via the Siemens SHELXTL computer software package.[21] Positions for most non-hydrogen atoms were visible on the initial E-map with positions of the remaining atoms found on subsequent electron density difference maps. Refinements proceeded normally (anisotropic thermal parameters for all non-hydrogen atoms). Hydrogen atom positions were calculated and isotropic thermal parameters were fixed at 0.08 Å^2 for **III** while for **VIIb** common isotropic parameters were refined initially but fixed in the last stage of refinement. Structure determinations of **I**, **VI**, and **VIIa** were also performed but were of lower quality than those of **III** and **VIIb** while at the same time showing no exceptional differences with these two structures. Hence full reports of these structure determinations have been deposited. Data collection and structure solution parameters and conditions are listed in Table 1 and atomic positions are listed in Tables 2 and 3 for structures **III** and **VIIb**. Selected bond lengths and angles are listed collectively for **I**, **III**, **VI**, **VIIa**, and **VIIb** in Table 4.

Dark green crystals of **X** were obtained from acetonitrile solution. Despite an extensive search, all the crystals mounted for X-ray analysis were found to diffract too weakly for a detailed crystal structure determination within contemporary standards. Several further attempts to grow crystals more suitable for X-ray diffraction studies have also been unsuccessful. Since the structure of this compound is of considerable interest in terms of elucidating the physical properties of oxo-bridged metal dimers, we decided to collect data on the best obtainable crystal in the hope of gleaning some useful information. An irregularly shaped crystal was sealed in a Lindemann glass capillary and mounted on a Siemens P4 diffractometer. Cell constants were obtained by least-squares refinement of the angular settings of 22 reflections in the range $10 < 2\theta < 22°$. Analysis of systematic absences lead to unambiguous identification of the space group. Structure solution via the Patterson method resulted in an electron density map in which the positions for all but a few of the non-hydrogen atoms were clearly visible. Final refinement was achieved with a model in which (1) the phenyl rings were constrained to an ideal geometry, (2) four possible orientations of a disordered acetonitrile solvate were identified and fixed, (3) anisotropic thermal parameters were refined only for vanadium and phosphorus, (4) hydrogen atom positions were calculated to give an ideal geometry and fixed to ride on their bound atoms, and (5) hydrogen atom thermal parameters were fixed at 0.08 Å^2. Data collection and structure solution/refinement parameters and conditions are listed in Table 1, atomic positions in Table 5, and selected bond lengths and angles in Table 4.

A red crystal of **XI** was prepared for X-ray diffraction studies as described above. Structure solution was achieved via direct methods with block-diagonal least-squares refinement ultimately required because of the large number of parameters. Disorder of the triflate anion and two of the solvent molecules reduced the overall accuracy of the structure, but the metrical data for the divanadium complex itself are unambiguous. The disordered triflate anion was refined constrained to an ideal geometry as were the disordered solvents, one THF and one toluene molecule, both with inversion generated disorder. With the two nondisordered THF solvent molecules there are a total of 2.5 THF and 0.5 toluene molecules per asymmetric unit. Data collection and structure solution/refinement parameters and conditions are listed in Table 1, atomic coordinates are listed in Table 6, and selected bond lengths and angles are listed in Table 4.

Results

Synthesis. The deep green, bent (μ-oxo)bis(μ-carboxylato)-divanadium(III) complexes can be prepared by a number of routes including the hydrolysis of mononuclear precursors such as $LV(DMF)Cl_2$, L = $HB(pz)_3^-$, or via preformed linear V−O−V cores. The latter method[22] proceeds readily in both aqueous solution via $[(H_2O)_5V{-}O{-}V(H_2O)_5]^{4+}$ or in organic solvents (i.e. DMF or acetonitrile) via a dark purple, linear, $[LV{-}O{-}VL]^{2+}$ intermediate. Attempts to prepare complexes with trispyrazolylborate groups with 3-, 4-, or 5-position substituents other than H or methyl invariably met with failure. Although the linear oxo-bridged intermediate seemed to form, as evidenced by the dark purple color, the failure to change color to green upon addition of acetate or other carboxylate suggests some steric interferences in forming the bent dimers

(21) Sheldrick, G. M. *SHELXTL-PC, Version 4.1*; Siemens X-ray Instruments, Inc.: Madison, WI, 1989. Scattering factors from: *International Tables for Crystallography*; Ibers, J., Hamilton, W., Eds.; Kynoch: Birmingham, England, 1974; Vol. IV.

(22) (a) Dave, B. C., Ph. D. Dissertation, University of Houston, 1993. (b) Dave, B. C.; Yan, Q.; Czernuszewicz, R. S. To be submitted for publication.

Table 2. Atomic Coordinates ($\times 10^4$) and Equivalent Isotropic Displacement Coefficients ($Å^2 \times 10^3$) for $[V_2O(O_2CH_2CH_3)_2(HB(pz)_3)_2]\cdot 4CH_3CN$ (**III**)

atom	*x*	*y*	*z*	*U*(eq)[a]
V(1)	4205(1)	344(1)	2473(1)	45(1)
V(2)	6141(1)	1650(1)	2501(1)	43(1)
N(1)	8493(5)	1561(4)	3109(3)	54(3)
N(2)	7551(5)	1354(4)	3194(3)	53(3)
N(3)	6891(4)	2902(4)	2517(3)	48(2)
N(4)	7908(5)	2944(4)	2516(3)	51(3)
N(5)	7959(4)	1570(4)	1928(3)	52(3)
N(6)	6916(5)	1368(4)	1821(3)	48(2)
N(7)	4571(4)	−718(4)	3120(3)	53(3)
N(8)	4001(5)	−1456(4)	3022(3)	54(3)
N(9)	3950(4)	−650(4)	1776(3)	53(3)
N(10)	3467(5)	−1413(4)	1846(3)	57(3)
N(11)	2588(5)	32(4)	2453(3)	53(3)
N(12)	2290(4)	−817(4)	2441(3)	51(3)
O(1)	5497(3)	635(3)	2485(2)	44(2)
O(2)	4908(4)	2164(3)	1823(3)	62(2)
O(3)	3573(4)	1276(3)	1808(3)	57(2)
O(4)	5538(4)	2127(3)	3180(3)	60(2)
O(5)	4234(4)	1211(3)	3176(3)	57(2)
C(1)	3763(8)	3101(7)	795(5)	106(6)
C(2)	3255(7)	2467(6)	1112(4)	78(4)
C(3)	3967(6)	1922(5)	1621(4)	53(3)
C(4)	4810(6)	1865(6)	3389(4)	56(3)
C(5)	4608(7)	2345(7)	3927(4)	81(4)
C(6)	5381(11)	2966(10)	4251(6)	167(9)
C(7)	7760(7)	951(6)	3745(4)	65(4)
C(8)	8831(7)	908(6)	4027(4)	81(4)
C(9)	9253(6)	1294(6)	3607(4)	75(4)
C(10)	6567(7)	3726(5)	2500(4)	64(4)
C(11)	7362(8)	4294(6)	2509(4)	78(5)
C(12)	8185(7)	3791(6)	2518(4)	67(4)
C(13)	8268(7)	1314(6)	1432(5)	72(4)
C(14)	7449(8)	940(7)	1009(4)	82(5)
C(15)	6629(7)	977(5)	1261(4)	59(3)
C(16)	1781(6)	489(5)	2479(4)	61(4)
C(17)	922(6)	10(6)	2453(5)	77(4)
C(18)	1289(6)	−836(6)	2430(4)	67(4)
C(19)	5304(6)	−823(6)	3675(4)	64(4)
C(20)	5212(8)	−1632(7)	3913(5)	82(5)
C(21)	4386(7)	−2018(6)	3493(5)	73(4)
C(22)	4191(6)	−720(6)	1239(4)	64(4)
C(23)	3879(7)	−1521(7)	960(5)	78(4)
C(24)	3420(7)	−1935(6)	1353(4)	72(4)
C(25)	1917(10)	5027(9)	886(6)	137(8)
C(26)	1564(12)	4669(11)	288(7)	130(8)
B(1)	8516(8)	2077(7)	2521(5)	68(4)
B(2)	3064(7)	−1541(6)	2424(5)	61(4)

[a] Equivalent isotropic *U* defined as one-third of the trace of the orthogonalized U_{ij} tensor.

Table 3. Atomic Coordinates ($\times 10^4$) and Equivalent Isotropic Displacement Coefficients ($Å^2 \times 10^3$) for $[V_2(OH)(O_2CH_2CH_3)_2(HB(pz)_3)_2](CF_3SO_3)\cdot C_4H_8O$ (**VIIb**)

atom	*x*	*y*	*z*	*U*(eq)[a]
V(1)	1320(1)	9406(1)	7947(1)	34(1)
V(2)	3423(1)	9050(1)	6891(1)	37(1)
O(1)	2551(4)	9776(4)	7432(3)	36(2)
O(11)	812(5)	8681(4)	7203(3)	45(2)
O(12)	2131(6)	8566(4)	6454(3)	50(3)
C(11)	1184(10)	8468(6)	6644(5)	40(4)
C(12)	402(9)	8086(7)	6173(5)	60(5)
C(13)	−755(11)	8212(9)	6313(7)	109(7)
O(21)	2169(6)	8475(4)	8343(3)	46(3)
O(22)	3417(6)	8169(3)	7577(3)	48(3)
C(21)	2936(8)	8040(6)	8116(5)	37(4)
C(22)	3299(9)	7302(6)	8509(4)	48(4)
C(23)	2770(9)	7177(6)	9192(5)	64(5)
N(111)	1651(7)	10206(5)	8736(3)	38(3)
N(112)	836(7)	10657(5)	9003(4)	39(3)
C(111)	2555(9)	10387(6)	9082(5)	46(4)
C(112)	2296(9)	10958(7)	9590(5)	49(4)
C(113)	1240(9)	11091(7)	9512(5)	45(4)
N(121)	−30(6)	9053(5)	8515(4)	37(3)
N(122)	−657(7)	9646(5)	8809(4)	36(3)
C(121)	−483(10)	8330(7)	8659(5)	53(5)
C(122)	−1384(10)	8443(8)	9029(5)	56(5)
C(123)	−1489(9)	9280(8)	9119(5)	54(5)
N(131)	284(6)	10332(4)	7584(4)	36(3)
N(132)	−342(6)	10779(4)	8012(4)	36(3)
C(131)	39(8)	10581(6)	6974(5)	47(4)
C(132)	−708(9)	11192(7)	6999(6)	62(5)
C(133)	−971(8)	11281(7)	7650(6)	54(4)
B(1)	−349(10)	10560(8)	8750(6)	46(5)
N(211)	4898(6)	9537(4)	7247(3)	38(3)
N(212)	5730(6)	9697(5)	6828(4)	44(3)
C(211)	5285(10)	9717(6)	7844(5)	53(4)
C(212)	6332(10)	10010(7)	7817(6)	61(5)
C(213)	6583(9)	9987(6)	7169(6)	59(4)
N(221)	4379(7)	8293(5)	6289(4)	46(3)
N(222)	5288(8)	8613(5)	5985(4)	47(3)
C(221)	4360(10)	7504(7)	6126(5)	57(5)
C(222)	5207(12)	7291(9)	5724(6)	71(6)
C(223)	5796(10)	7989(9)	5649(5)	63(5)
N(231)	3590(7)	9918(5)	6131(3)	42(3)
N(232)	4586(7)	10066(5)	5857(4)	40(3)
C(231)	2914(9)	10432(7)	5846(5)	56(5)
C(232)	3425(11)	10919(7)	5386(5)	63(5)
C(233)	4489(12)	10675(7)	5419(5)	60(5)
B(2)	5535(11)	9542(9)	6072(6)	55(5)

[a] Equivalent isotropic *U* defined as one-third of the trace of the orthogonalized U_{ij} tensor.

from linear ones with highly substituted pyrazoles. While the (μ-oxo)bis(μ-phosphato) complex can also be obtained, albeit in very poor yield, via direct reaction as above, it proceeds more readily via ligand exchange with the μ-carboxylato complexes, presumably via proton transfer.

Description of Structures. A. $[V_2O(O_2CH_2CH_3)_2(HB(pz)_3)_2]\cdot 4CH_3CN$ (III). The structure of compound **III**, shown in Figure 1 with atom labels, is typical of supported μ-oxo-bridged *M*(III) dinuclear complexes. The complex contains no formal symmetry, but the core structure conforms closely to C_{2v} point symmetry with one symmetry plane containing the V−O−V angle and the other bisecting it. The metrical data for this complex is comparable to that of the bis(μ-acetato) analog, **I**, as can be seen by perusing Table 4, indicating that substitution of the carboxylate bridge leaves the core structure relatively unchanged. The coordination environment about each metal center is distorted octahedral with the bond to the bridging oxygen significantly shorter than the others [mean values (Å): $V-O_{oxo} = 1.778(5)$, $V-O_{carboxylate} = 2.046(6)$, $V-N_{cis} = 2.12(1)$, $V-N_{trans} = 2.18(3)$] suggesting a strong π interaction between the metal and the μ-oxo group. The one notable difference between the structure of **III** and all previously reported species with various trivalent metals is the V−O−V angle (133.3°) which is about 10° larger than the *M*−O−*M* angle found in the latter group.[23-25]

B. $[V_2(OH)(O_2CH_2CH_3)_2(HB(pz)_3)_2](CF_3SO_3)\cdot$THF (VIIb). The structure of **VIIb**, shown in Figure 2 with atom labels, is very similar to the reported structures of related *M*(III) dinuclear complexes. The primary differences between **VIIb** and **III** are the increase in $V-O_{oxo}$ bond length [to 1.934(2) Å] and the simultaneous decrease in V−O−V angle [to 123.5(3)°] that accompanies protonation. The change in bond length is expected since the increase in coordination of the bridging

(23) (a) Armstrong, W. H.; Lippard, S. J. *J. Am. Chem. Soc.* **1983**, *105*, 4837. (b) Wiegahrdt, K.; Pohl., J.; Gebrt, W. *Angew.Chem., Int. Ed. Engl.* **1983**, *22*, 727.

(24) Sheats, J. E.; Czernuszewicz, R. S.; Dismukes, G. C.; Rheingold, A. L.; Petrouleas, V.; Stubbe, J.; Armstrong, W. H.; Beer, R. H.; Lippard, S. J. *J. Am. Chem. Soc.* **1987**, *109*, 1435.

Table 4. Selected Bond Lengths (Å) and Angles (deg) for **I**, **III**, **VI**, **VIIa**, **VIIb**, **X**, and **XI** where Atom Numbering Scheme refers to Universal Scheme Below for Core Atoms of the Dimer

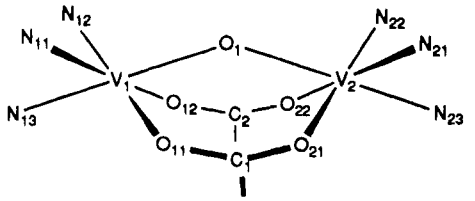

bond length/angle	I	III	VI	VIIa	VIIb	X	XI
V(1)−O(1)−V(2)	134.7 (6)	133.3 (3)	122.9 (3)	123.4 (4)	123.5 (3)	143.7 (13)	133.1 (5)
V(1)−O(1)	1.761(10)	1.781(5)	1.927(5)	1.942(8)	1.935(6)	1.790(20)	1.961(9)
V(2)−O(1)	1.779(10)	1.774(5)	1.946(5)	1.932(8)	1.932(6)	1.795(25)	1.957(9)
V(1)−O(11)	2.051(8)	2.053(5)	1.989(7)	1.999(11)	2.003(7)	2.065(24)	2.023(8)
V(1)−O(12)	2.051(8)	2.043(6)	1.993(6)	1.983(10)	2.009(7)	2.084(27)	2.029(12)
V(1)−N(11)	2.097(10)	2.126(7)	2.072(7)	2.068(13)	2.096(8)	2.104(33)	2.079(16)
V(1)−N(12)	2.097(10)	2.132(6)	2.101(8)	2.117(12)	2.101(8)	2.110(29)	2.081(10)
V(1)−N(13)	2.170(14)	2.207(7)	2.101(7)	2.107(12)	2.099(8)	2.155(32)	2.076(14)
O(1)−V(1)−O(11)	91.5(3)	92.0(2)	93.3(2)	91.9(4)	92.3(3)	91.6(10)	91.4(3)
O(1)−V(1)−O(12)	91.5(3)	91.2(2)	92.8(2)	92.4(4)	91.2(3)	90.9(10)	92.1(4)
O(1)−V(1)−N(11)	98.9(4)	98.2(2)	92.6(3)	92.2(4)	93.8(3)	101.2(11)	93.9(5)
O(1)−V(1)−N(12)	98.9(4)	98.4(2)	92.2(3)	95.5(4)	93.7(3)	98.7(12)	90.2(4)
O(1)−V(1)−N(13)	177.3(5)	178.0(2)	175.7(3)	176.3(4)	177.8(3)	176.2(13)	173.5(4)
O(11)−V(1)−O(12)	89.2(5)	90.7(2)	90.8(3)	89.8(4)	91.3(3)	91.6(10)	89.4(4)
O(11)−V(1)−N(11)	91.7(4)	91.6(2)	91.7(3)	90.6(5)	93.4(3)	87.6(11)	89.6(5)
O(11)−V(1)−N(12)	169.6(4)	169.2(2)	174.4(3)	172.5(4)	174.0(3)	169.6(11)	175.9(5)
O(11)−V(1)−N(13)	86.6(3)	86.3(2)	90.2(3)	89.1(5)	89.4(3)	87.2(11)	95.1(4)
O(12)−V(1)−N(11)	169.6(4)	170.3(3)	173.8(3)	175.3(4)	173.0(3)	167.9(12)	174.0(5)
O(12)−V(1)−N(12)	91.7(4)	91.7(2)	89.8(3)	91.0(5)	88.0(3)	89.9(11)	94.2(5)
O(12)−V(1)−N(13)	86.6(3)	87.6(2)	89.6(3)	91.1(4)	90.3(3)	85.5(12)	88.4(5)
N(11)−V(1)−N(12)	85.6(6)	84.4(2)	87.2(3)	87.9(5)	86.8(3)	88.8(12)	86.5(5)
N(11)−V(1)−N(13)	83.1(4)	83.1(2)	84.7(3)	84.2(5)	84.6(3)	82.3(13)	85.7(6)
N(12)−V(1)−N(13)	83.1(4)	83.3(2)	84.2(3)	83.5(5)	84.6(3)	87.2(12)	83.3(5)
V(2)−O(21)	2.035(9)	2.046(5)	1.994(7)	1.969(11)	1.989(6)	2.008(23)	2.036(8)
V(2)−O(22)	2.035(9)	2.040(6)	2.006(6)	1.984(10)	1.982(7)	2.053(27)	2.019(10)
V(2)−N(21)	2.104(11)	2.109(7)	2.093(7)	2.089(11)	2.106(8)	2.060(29)	2.090(14)
V(2)−N(22)	2.104(11)	2.114(6)	2.069(7)	2.088(12)	2.093(8)	1.987(34)	2.090(13)
V(2)−N(23)	2.172(15)	2.159(6)	2.069(7)	2.078(12)	2.091(9)	2.158(36)	2.081(12)
O(1)−V(2)−O(21)	91.5(3)	92.1(2)	92.5(2)	92.4(4)	92.3(3)	92.1(10)	90.2(4)
O(1)−V(2)−O(22)	91.5(3)	91.9(2)	92.1(2)	90.7(4)	92.8(3)	91.9(11)	90.8(4)
O(1)−V(2)−N(21)	99.0(3)	98.3(2)	92.9(2)	96.2(4)	93.3(3)	100.6(12)	91.8(5)
O(1)−V(2)−N(22)	99.0(3)	98.9(2)	92.9(3)	93.2(4)	93.6(3)	99.5(13)	95.3(4)
O(1)−V(2)−N(23)	176.9(5)	178.6(2)	178.1(3)	176.7(4)	178.3(3)	174.5(12)	176.9(5)
O(21)−V(2)−O(22)	89.4(5)	89.9(2)	90.6(2)	90.9(4)	91.4(3)	87.7(10)	91.6(4)
O(21)−V(2)−N(21)	90.6(4)	90.7(2)	91.9(3)	91.0(5)	91.9(3)	91.6(10)	92.8(4)
O(21)−V(2)−N(22)	169.5(4)	169.0(2)	174.2(3)	174.1(4)	173.6(3)	168.3(13)	174.4(4)
O(21)−V(2)−N(23)	86.3(4)	86.8(2)	89.2(3)	90.6(5)	89.3(3)	86.7(11)	88.8(4)
O(22)−V(2)−N(21)	169.5(4)	169.8(2)	174.4(3)	172.7(5)	173.0(3)	167.6(12)	174.9(5)
O(22)−V(2)−N(22)	90.6(4)	90.0(2)	91.3(3)	90.9(4)	90.9(3)	92.9(12)	89.5(5)
O(22)−V(2)−N(23)	86.3(4)	87.2(2)	88.7(3)	87.8(5)	87.7(3)	82.8(12)	92.2(5)
N(21)−V(2)−N(22)	87.5(6)	87.5(2)	85.8(3)	86.5(4)	85.1(3)	85.3(13)	85.9(5)
N(21)−V(2)−N(23)	83.3(4)	82.6(2)	86.2(3)	85.2(5)	86.2(3)	84.8(12)	85.3(5)
N(22)−V(2)−N(23)	83.3(4)	82.2(2)	85.4(3)	83.9(5)	84.8(3)	81.8(14)	85.6(5)

oxygen upon protonation should reduce the strength of the metal-oxygen bonds. However, the change in bond angle is notable since the *M*−O−*M* bridge angle in *M*(III) systems other than V(III) changes little upon protonation. Thus the bridge angle in the protonated V(III) systems is reduced to conform to the values found in both unprotonated and protonated complexes of analogous trivalent metal dimers.[1,2,23−25] The similarity in the metrical parameters of **VIIb** with those of the other two protonated V(III) complexes, **VI** and **VIIa**, reported here (cf. Table 4) demonstrates that the core geometry is not affected greatly by changes in bridging carboxylates, counterions, or cocrystallized solvent molecules. The last point does bring up another interesting feature of these compounds, however. In each structure a single cocrystallized solvent molecule (CH_3CN in **VI** and **VIIa** and THF in **VIIb**) is found with a nitrogen or oxygen atom hydrogen-bonded to the proton of the μ-hydroxo bridge of the dinuclear complex (we have also observed a hydrogen bonding interaction to a $(C_2H_5)_2O$ solvate molecule in a partially refined structure of the benzoate analog, **II**[26]). The hydrogen bonding appears to be strongest for the THF solvate, as it is the shortest (O···H = 1.63 Å) and straightest (O···H−O = 178°) of the bonds, which would account for its

(25) (a) Martin, L. L.; Wieghardt, K.; Blodin, G.; Girerd, J.-J.; Nuber, B.; Weiss, J. *J. Chem. Soc. Chem. Commun.* **1990**, 1767. (b) Neubold, P.; Wieghardt, K.; Nuber, B.; Weiss, J. *Angew. Chem., Int. Ed. Engl.* **1988**, *27*, 933. (c) Wiegahrdt, K.; Bossek, U.; Nuber, B.; Weiss, J.; Bonvoisin, J.; Corbella, M.; Vitols, S. E.; Girerd, J.-J. *J. Am. Chem. Soc.* **1988**, *110*, 7398. (d) Hartman, J. R.; Radin, R. L.; Chaudhuri, P.; Pohl, K.; Wieghardt, K.; Nuber, B.; Weiss, J.; Papaefthymiou, G. C.; Frankel, R. B.; Lippard, S. J. *J. Am. Chem. Soc.* **1987**, *109*, 7387. (e) Wieghardt, K.; Bossek, U.; Ventur, D.; Weiss, J. *J. Chem. Soc., Chem. Commun.* **1985**, 347. (f) Wu, F. -J.; Kurtz, D. M., Jr.; Hagen, K. S.; Nyman, P. D.; Debrunner, P. G.; Vankai, V. A. *Inorg. Chem.* **1990**, *29*, 5174.

(26) Bond, M. R.; Verastegue, R., Carrano, C. J. Unpublished work, 1993.

Table 5. Atomic Coordinates ($\times 10^4$) and Equivalent Isotropic Displacement Coefficients ($Å^2 \times 10^3$) for $[V_2O(O_2P(OC_6H_5)_2(HB(pz)_3)_2]\cdot CH_3CN$ (**X**)

atom	*x*	*y*	*z*	*U*(eq)[a]
V(1)	2232(6)	351(3)	1738(3)	39(3)
V(2)	1724(7)	1340(3)	2959(3)	44(3)
P(1)	186(11)	72(7)	2605(6)	46(6)
P(2)	692(11)	1672(6)	1565(6)	41(6)
O(1)	2429(18)	824(12)	2435(10)	31(8)
O(2)	459(21)	656(13)	3013(12)	50(9)
O(3)	765(21)	−67(12)	2028(11)	52(9)
O(4)	250(23)	−610(14)	2967(14)	76(10)
O(5)	−1116(26)	142(14)	2430(12)	77(10)
O(6)	781(18)	1772(11)	2265(11)	21(8)
O(7)	1343(20)	1117(11)	1295(11)	30(8)
O(8)	−567(26)	1622(14)	1249(13)	76(11)
O(9)	1149(23)	2363(12)	1323(12)	58(9)
B(1)	3859(38)	−561(22)	975(21)	27(16)
N(1)	3628(26)	656(16)	1274(14)	48(11)
N(2)	4347(29)	179(16)	1025(14)	45(11)
C(51)	4123(35)	1257(22)	1223(17)	56(15)
C(52)	5143(44)	1126(25)	924(21)	97(19)
C(53)	5100(42)	495(26)	780(21)	87(18)
N(3)	1880(31)	−225(16)	908(14)	57(12)
N(4)	2718(31)	−622(17)	643(17)	59(12)
C(54)	894(38)	−365(19)	583(18)	58(15)
C(55)	1244(36)	−820(19)	98(19)	47(14)
C(56)	2379(42)	−949(23)	136(23)	92(18)
N(5)	3131(25)	−511(14)	2029(14)	28(9)
N(6)	3845(24)	−808(15)	1623(14)	31(10)
C(57)	3141(37)	−857(23)	2557(21)	61(15)
C(58)	3843(31)	−1398(19)	2515(16)	33(13)
C(59)	4211(30)	−1380(20)	1947(17)	43(13)
B(2)	2612(43)	2213(26)	4170(24)	43(17)
N(7)	3105(26)	2450(15)	3603(15)	34(10)
N(8)	2795(24)	2145(14)	3032(13)	17(9)
C(61)	3748(35)	2988(19)	3529(19)	56(15)
C(62)	3940(32)	3011(19)	2883(18)	47(14)
C(63)	3376(32)	2489(21)	2630(20)	49(15)
N(9)	1261(30)	2209(16)	4050(17)	51(11)
N(10)	743(31)	1897(15)	3575(16)	46(11)
C(64)	503(36)	2509(20)	4460(20)	62(15)
C(65)	−503(37)	2344(19)	4145(19)	48(15)
C(66)	−317(42)	1999(20)	3651(21)	63(16)
N(11)	2853(28)	1427(17)	4246(16)	49(11)
N(12)	2508(27)	1046(17)	3751(16)	56(12)
C(67)	3375(34)	1125(20)	4718(21)	56(15)
C(68)	3447(34)	466(20)	4540(20)	55(15)
C(69)	2948(29)	424(20)	3959(17)	37(13)
C(2)	723(20)	−1142(13)	3925(15)	73(16)
C(3)	568	−1253	4546	120(21)
C(4)	−281	−919	4826	86(17)
C(5)	−976	−474	4485	91(18)
C(6)	−821	−362	3864	47(13)
C(1)	28	−697	3583	72(16)
C(12)	−2240(23)	−841(15)	2152(10)	65(15)
C(13)	−2795	−1235	1696	98(17)
C(14)	−2806	−1047	1078	59(15)
C(15)	−2261	−466	915	49(14)
C(16)	−1705	−73	1371	50(13)
C(11)	−1695	−260	1990	57(14)
C(22)	−1943(27)	1832(12)	2001(14)	61(15)
C(23)	−2882	2202	2136	177(28)
C(24)	−3279	2709	1739	87(18)
C(25)	−2736	2847	1208	140(24)
C(26)	−1797	2478	1073	92(18)
C(21)	−1400	1970	1470	71(17)
C(32)	1229(23)	3192(16)	597(14)	90(18)
C(33)	1296	3445	3	100(20)
C(34)	1301	3012	−498	78(17)
C(35)	1238	2326	−407	82(18)
C(36)	1171	2073	187	105(19)
C(31)	1166	2506	689	97(13)

[a] Equivalent isotropic *U* defined as one-third of the trace of the orthogonalized $\mathbf{U}_{ij}$ tensor.

Table 6. Atomic Coordinates ($\times 10^4$) and Equivalent Isotropic Displacement Coefficients ($Å^2 \times 10^3$) for $[V_2(OH)(O_2P(OC_6H_5)_2)_2(HB(pz)_3)_2](CF_3SO_3)\cdot 2.5C_4H_8O\cdot 0.5C_6H_5CH_3$ (**XI**)

atom	*x*	*y*	*z*	*U*(eq)[a]
V(1)	1550(2)	3131(2)	2596(1)	43(1)
V(2)	2420(2)	761(2)	2731(1)	41(1)
P(1)	387(4)	1728(3)	1981(2)	47(2)
P(2)	593(4)	1371(3)	3980(2)	44(2)
O(1)	2612(8)	2119(6)	2498(4)	41(4)
O(2)	1055(7)	931(6)	2291(5)	42(4)
O(3)	417(8)	2605(7)	2198(5)	59(5)
O(4)	−898(8)	1445(6)	2152(5)	50(4)
O(5)	821(9)	1928(7)	1148(5)	60(5)
O(6)	1431(8)	723(6)	3709(5)	47(4)
O(7)	768(8)	2376(6)	3596(5)	44(4)
O(8)	−612(8)	1003(6)	4012(5)	51(4)
O(9)	518(8)	1203(7)	4800(5)	55(5)
B(1)	2336(18)	5302(14)	2144(10)	58(8)
N(1)	2660(12)	4887(9)	1510(6)	59(6)
N(2)	2392(11)	3975(9)	1599(6)	52(5)
C(51)	3292(16)	4617(13)	469(10)	86(8)
C(52)	2771(14)	3836(13)	955(9)	71(8)
C(53)	3187(16)	5265(12)	862(10)	72(8)
N(3)	1010(13)	5170(9)	2401(7)	61(6)
N(4)	527(12)	4291(9)	2586(6)	55(6)
C(54)	199(19)	5786(12)	2427(9)	75(8)
C(55)	−839(19)	5346(14)	2605(10)	89(9)
C(56)	−572(17)	4429(13)	2690(9)	76(8)
N(5)	2835(12)	4710(10)	2732(7)	61(6)
N(6)	2580(10)	3770(9)	3028(7)	49(6)
C(57)	3099(14)	3459(12)	3565(9)	59(7)
C(58)	3767(15)	4183(13)	3616(10)	76(8)
C(59)	3528(16)	4931(12)	3088(10)	69(8)
B(2)	4371(17)	−726(13)	2489(10)	54(8)
N(7)	3901(10)	523(9)	3120(6)	48(5)
N(8)	4620(11)	−157(9)	2996(6)	50(6)
C(61)	5486(14)	−197(11)	3282(9)	57(7)
C(62)	5343(15)	485(12)	3630(10)	73(8)
C(63)	4339(15)	892(11)	3524(8)	59(7)
N(9)	2274(12)	−693(8)	3017(7)	52(6)
N(10)	3189(11)	−1212(9)	2847(7)	53(6)
C(64)	2873(16)	−2114(11)	3036(9)	69(8)
C(65)	1731(15)	−2182(11)	3323(10)	70(8)
C(66)	1380(15)	−1302(10)	3318(8)	58(7)
N(11)	3441(10)	656(9)	1765(7)	50(6)
N(12)	4252(11)	−17(9)	1789(7)	49(6)
C(67)	4805(15)	51(13)	1106(10)	70(8)
C(68)	4368(17)	784(12)	660(9)	74(8)
C(69)	3509(15)	1125(11)	1076(8)	64(7)
C(2)	−1609(10)	503(8)	1548(5)	78(8)
C(3)	−1964	−370	1546	102(9)
C(4)	−1969	−1151	2136	102(9)
C(5)	−1618	−1059	2729	90(8)
C(6)	−1263	−186	2731	64(7)
C(1)	−1258	595	2141	62(7)
C(12)	−317(10)	3319(9)	744(5)	76(8)
C(13)	−694	3947	178	103(9)
C(14)	−370	3844	−509	149(11)
C(15)	331	3112	−630	179(11)
C(16)	709	2483	−64	126(10)
C(11)	384	2587	623	62(7)
C(22)	−2114(9)	1279(7)	4943(5)	59(7)
C(23)	−3145	1690	5149	75(8)
C(24)	−3662	2276	4630	74(8)
C(25)	−3146	2449	3905	84(8)
C(26)	−2115	2037	3699	65(7)
C(21)	−1599	1452	4218	52(6)
C(32)	1099(9)	2416(8)	5195(5)	74(8)
C(33)	1902	2833	5414	92(9)
C(34)	2944	2408	5465	97(9)
C(35)	3182	1567	5297	83(8)
C(36)	2379	1150	5078	65(7)
C(31)	1337	1575	5026	50(6)

[a] Equivalent isotropic *U* defined as one-third of the trace of the orthogonalized $\mathbf{U}_{ij}$ tensor.

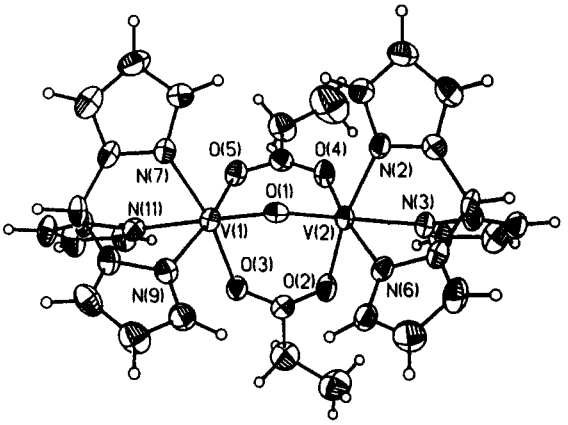

Figure 1. Thermal ellipsoid plot (30%) showing the atom-labeling scheme for **III.**

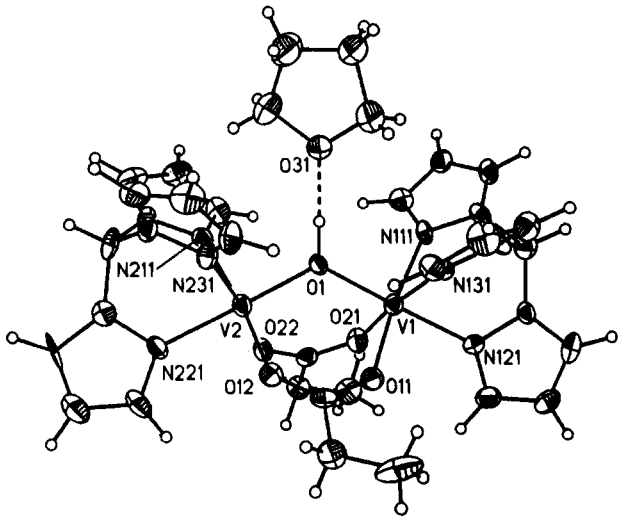

Figure 2. Thermal ellipsoid plot (30%) showing the atom-labeling scheme for **VIIb.**

preferential crystallization from a CH_3CN/THF mixture. In spite of this close interaction with the bridging hydroxo group, core geometries of the complex are remarkably similar among the three structures of protonated complexes reported here.

C. $[V_2O(O_2P(OC_6H_5)_2)_2(HB(pz)_3)_2]\cdot CH_3CN$ (X). Given the limitations imposed by the lack of data, the structure obtained for the bis(μ-phosphato) complex, **X** (Figure 3), is surprisingly detailed. Although the reported esd's do not allow a rigorous analysis of the bonding within the dimer, the stereochemical arrangement of the dimer is well-defined and the metrical data of the dimetallic core are unambiguous. The core bonding geometry correlates well with that found for the bis(μ-carboxylato) systems [mean value (Å): $V-O_{oxo} = 1.79(2)$, $V-O_{phosphate} = 2.05(3)$, $V-N_{cis} = 2.07(6)$ Å, and $V-N_{trans} = 2.16(3)$] but the V···V distance [3.406(11) Å] and V−O−V bridge angle [143.7(13)°] are significantly larger in the latter.

D. $[V_2(OH)(O_2P(OC_6H_5)_2)_2(HB(pz)_3)_2](CF_3SO_3)\cdot 2.5THF\cdot 0.5C_6H_5CH_3$ (XI). The major changes associated with protonation of the oxo-bridge in **X** to yield **XI** (shown in Figure 4 with atom labels) are the expected lengthening of the $V-O_{oxo}$ bond length to 1.959(10) Å and a decrease in the V−O−V angle to 133.1(5)° (Table 4). These changes mirror those seen for the μ-O(H)bis(μ-carboxylato) complexes discussed above. In this case, however, the "bite" of the cobridging phosphate ligands allows the formally sp hybridized oxo bridge in **X** to open up to 143.7(13)°, thereby maximizing π bonding, while restricting the sp^2 hybridized hydroxo oxygen in **XI** to 133.1(5)° rather than the ideal 120°. The V−O(H)−V angle found

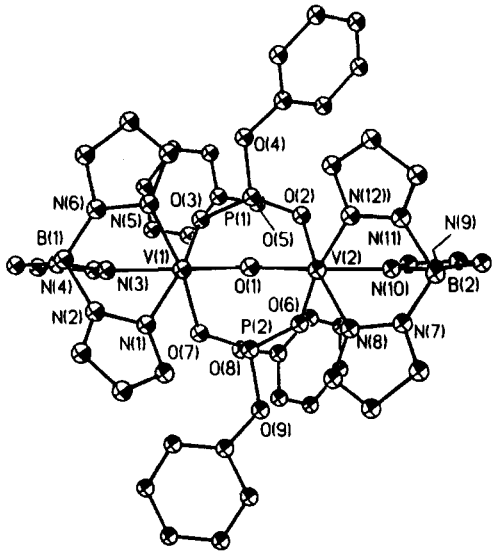

Figure 3. Thermal ellipsoid plot (30%) showing the atom-labeling scheme for **X.**

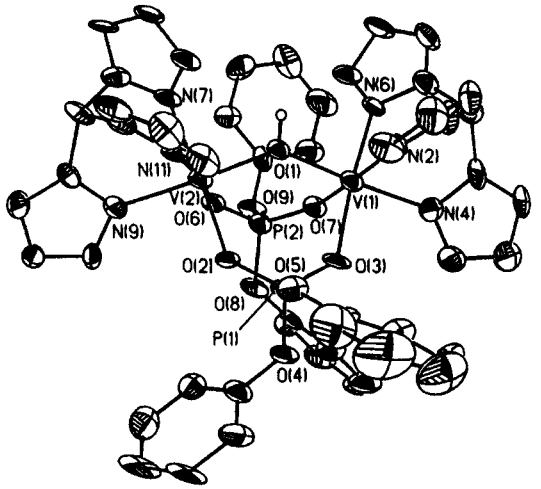

Figure 4. Thermal ellipsoid plot (30%) showing the atom-labeling scheme for **XI.**

for complex **XI** also agrees with the Fe−O−Fe angle [134.7(3)°] found in a (μ-oxo)bis(μ-phosphato) diferric complex reported by Armstrong and Lippard.[27]

Electrochemistry. In contrast to the corresponding cationic (μ-oxo)bis(μ-acetato)divanadium(III) complexes with the tacn ligand reported by Wieghardt,[11] none of the neutral hydridotris(pyrazolyl)borate complexes show evidence for quasi-reversible electrochemical behavior in DMF, acetonitrile, or CH_2Cl_2 over a potential range of ±1.5 V. Rather they display irreversible oxidations with $E_a = +0.12$ V for the acetate (**I**), $E_a = +0.14$ V for the phosphate (**X**), and $E_a = +0.15$ and +0.76 V for the benzoate (**II**) with product waves in all cases observable near −0.5 V. Upon protonation with perchloric acid, however, the irreversible oxidation waves disappear with the concomitant appearance of two quasi-reversible reductions with $E° = -0.40$ and −1.03 V for the acetate (**VI**) and −0.55 and −0.95 V for the phosphate (**XI**), one quasi-reversible couple at −0.48 V, and an irreversible reduction wave at −1.1 V for the benzoate (**VIII**). Since from simple charge considerations the neutral species pick up a positive charge upon protonation, oxidations should become more difficult while reductions should be more facile, as is observed. Furthermore, protonation of the oxo

(27) Armstrong, W. H.; Lippard, S. J. *J. Am. Chem. Soc.* **1985**, *107*, 3730.

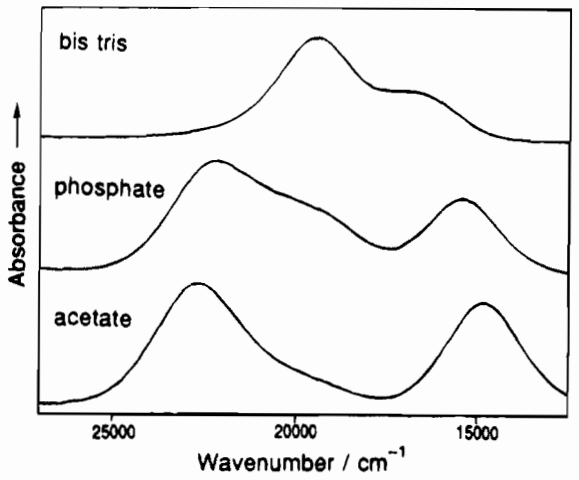

Figure 5. UV−visible spectra of **I**, **X**, and $[V_2O(HB(pz)_3)_2(H_2Bpz_2)_2]$ in acetonitrile.

group, a good π donor, to a hydroxide should also favor the lower oxidation state.

UV−Visible Spectroscopy. The electronic spectra of all the oxo-bridged compounds are very similar to one another and to the analogous tacn complexes.[11] These electronic spectra (Figure 5) display intense maxima ($\epsilon_m > 2000$ M^{-1} cm^{-1}) in the visible region (440−450 and 665−690 nm) which appear to be characteristic of the (μ-oxo)bis(μ-carboxylato or phosphato) core. It has generally been assumed that these transitions arise from ligand-to-metal charge transfer involving the bridging oxo group. This is consistent with both the intensity of these transitions and the fact that the cationic tacn complexes display their maxima at lower energy than the neutral tris(pyrazolyl)borates.[10,11] Final confirmation of this assignment comes from resonance Raman spectroscopy (*vide infra*).

Protonation of the dark-green (μ-oxo)bis(μ-carboxylato or phosphato) complexes with $HClO_4$ in acetonitrile results in a rapid color change to pale pink with a concomitant bleaching of the ~440 and ~665 nm bands. Upon protonation new, weak, d−d transitions are observed at 515 and 715 nm for the acetate (**VI**) and at 520 and 730 nm for the benzoate (**VIII**) analogs. The process is reversible and an isobestic point is maintained during the titration indicating a simple protonation/deprotonation reaction. Analysis of absorbance vs "pH" in acetonitrile solution gives an apparent pK_a near 3.0 for both the acetate (**VI**) and the benzoate (**VIII**) and 3.8 for the phosphate (**XI**). Correcting for the difference in solvents, these values are very similar to those reported by Wieghardt *et al.* for the corresponding tacn complexes.[11] The X-ray structure reveals that, as expected, the site of protonation is the oxo bridge (*vide supra*).

Paramagnetic NMR Spectroscopy. Although the electronic properties of V(III) are often favorable for the observation of paramagnetically shifted ligand proton resonances, few such spectra have been reported.[28,29] However, since particularly well resolved spectra have been observed for the corresponding Mn(III) and Fe(III) (μ-oxo)bis(μ-carboxylato) bridged species, we attempted to record them for the V(III) complexes as well. Figure 6 shows the proton NMR spectra of $[V_2O(O_2CCH_3)_2(HB(pz)_3)_2]$ (**I**) which consists of at least seven identifiable resonances over the range of +81 to −50 ppm. This range is larger than that observed for the corresponding Mn(III)[24] and Fe(III)[25d] species. For example, the acetate resonances (as

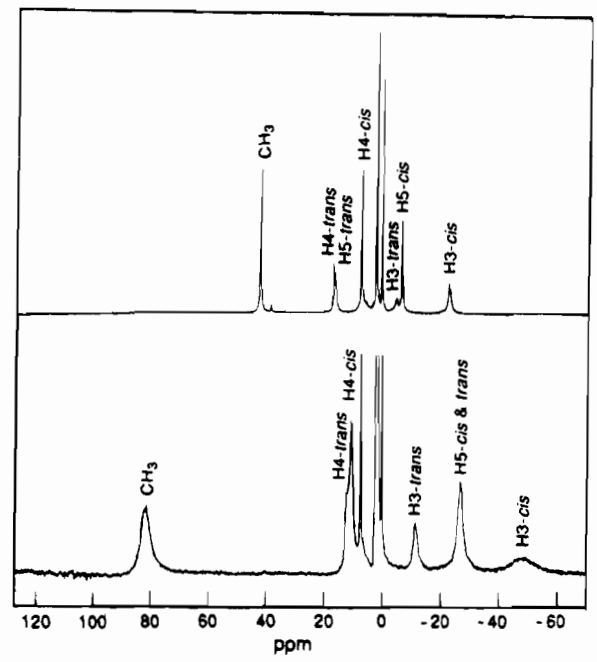

Figure 6. Paramagnetic NMR spectra for **I** (lower) and **VI** (upper).

assigned by selective deuteration) appear at +81 ppm for V(III), +66 ppm for Mn(III) and +10.5 ppm for Fe(III); however, these differences do not correspond simply to the ratios of the effective magnetic moments. The specific assignments of peaks is given in Table 7. Lines arising from the 3- and 5-position pyrazole protons were identified based on their absence in the hydridotris(3,5-dimethylpyrazolyl)borate analogs with the larger linewidth peak assigned to the position closer to the paramagnetic center.[28,29] The identity of the peaks arising from the 4 position and the absence of a B−H proton resonance were all established by selective deuteration.

The pyrazole protons appear in two groups in a 2:1 ratio corresponding to the two pyrazole rings *cis* to the oxo bridge and the one pyrazole ring *trans* to the bridge. In the unprotonated complexes the shifts of both the *cis* and the *trans* pyrazole protons follow an alternating sign pattern around the ring with the 3- and 5-protons experiencing upfield shifts and the 4-protons a downfield shift. This is consistent with the results of an extended Hückel calculation on the monomeric fragment[30] which shows that the t_{2g} orbitals of the metal delocalize into ligand π orbitals containing significant admixture of the carbon p_z orbitals at the 3- and 5-positions but not at the 4. The net negative shift as well as the change in sign experienced when the 3- and 5-position protons are replaced by methyl groups are also consistent with a direct π delocalization pathway for the unpaired spin of the metal.[31] Upon protonation of the oxo bridge, two effects are observed in the paramagnetic NMR (Figure 6, top). The first is a reduction in the overall spread of the spectrum, which now is completely contained within ~60 ppm rather than the ~120 ppm seen with the unprotonated dimers. For example, the acetate methyl resonances appear at +41.9 ppm in the protonated complex and at +81.0 ppm in the unprotonated giving a ratio of $\Delta H_{\text{protonated}}/\Delta H_{\text{unprotonated}}$ of 0.52. If the dipolar contribution to these shifts is small, then, to a first approximation, this ratio should equal the ratio of the square

(28) Rohrschied, F.; Ernst, R. E.; Holm, R. H. *Inorg. Chem.* **1967**, *6*, 1315.
(29) Swift, T. J. In *NMR of Paramagnetic Molecules; Principles and Applications*, La Mar, G. N., Ed., Academic Press: New York, 1973; p 53.
(30) *Hyperchem Release 3 for Windows*; Autodesk, Inc.: Sausalito, CA 1993. Extended Hückel calculations were run using the crystallographically refined coordinates of the atoms of the complex and Hückel parameters embedded in the software.
(31) Boyd, D. W.; Hope, J.; Martin, R. L. *J. Chem. Soc., Dalton Trans.* **1986**, 887.

Table 7. Proton NMR Data (ppm) at 25 °C for Compounds **I**−**XII**

			Pyrazolylborate					
			cis			trans		
compound	bridging ligand	3(5)-methyl	H3	H4	H5	H3	H4	H5
			Oxo-Bridged[a]					
acetate, **I**	81.0 (CH_3)		−49.3	+10.6	−27.0	−11.5	+12.1	−27.0
propionate, **III**	84.0 (CH_2)		−47.9	+10.8	−26.5	−11.1	+12.1	−26.5
formate, **IV**			−49.7	+9.7	−28.6	−12.4	+9.7	−28.6
benzoate, **II**	−7.6, 1.2, 7.3 (Ph)[c]		−47.7	+10.9	−26.8	−10.9	+10.9	−26.8
acetate, **V**	69.5 (CH_3)	32.3		+8.9			+8.9	
			Hydroxo-Bridged[b]					
acetate, **I**	41.9 (CH_3)		−23.2	+7.1	−6.9	−4.9	+16.6	+16.0
propionate, **VII**	49.6 (CH_2)		−23.4	+7.1	−6.9	−4.9	+16.7	+16.0
formate, **IX**			−23.3	+6.6	−6.9	−4.8	+18.3	+16.6
benzoate, **VIII**	0.21, 1.1, 3.4, 8.9 (Ph)		−23.9	+6.8	−7.1	−5.0	+16.8	+16.8
phosphate, **XI**	3.4, 7.0, 7.2 (Ph)		−27.3	+7.9	−9.6	−11.5	+15.5	+13.8
acetate, **XII**	38.3 (CH_3)	24.7		+7.9			+13.9	

[a] In $CDCl_3$. [b] In CD_3CH. [c] Ph = C_6H_5.

of the effective magnetic moments of the two complexes, 0.57 in this case. The second is the large positive shift of the *trans* pyrazole ring proton resonances relative to those of the unprotonated complex. This large shift suggests a change in direct delocalization pathway for the *trans* pyrazole ring from one dominated by π interactions to one dominated by σ.

Resonance Raman Spectroscopy. The resonance Raman (RR) scattering with variable-wavelength excitation of tribridged oxo complexes **I** and **X** was examined in order to characterize the signature vibrations of the (μ-oxo)divanadium(III) core and the nature of the visible electronic absorption bands. A bent V−O−V moiety (C_{2v} symmetry) has three normal modes of vibration: A_1, B_2, and A_1, corresponding to a symmetric V−O−V stretch, ν_s(VOV), an asymmetric stretch, ν_{as}(VOV), and a bending mode, δ(VOV), respectively. All three can be observed in RR spectra excited with red (647.1, 676.4 nm) and violet (406.7−457.9 nm) laser lines, indicating that most of the intensity of the ~450- and ~675-nm absorption bands is due to oxo-to-vanadium(III) CT transitions (*vide infra*). The RR enhancement pattern of the V−O−V bridge vibrational modes is similar to those previously reported[22,24,32,33] for the isostructural $[Fe_2O(O_2CCH_3)_2(HB(pz)_3)_2]$[32] and $[Mn_2O(O_2CCH_3)_2(HB(pz)_3)_2]$[24] dimers.

Figure 7 compares the solid state RR spectra of $[V_2O(O_2CCH_3)_2(HB(pz)_3)_2]$ (**I**) and its ^{18}O isotopomer obtained at low temperature (77K) in the 100−1400 cm^{-1} region with excitation at 676.4 nm, in resonance with the 673-nm absorption band. The most intense band at 536 cm^{-1} in the RR spectra of the acetato complex **I**, which shifts to 520 cm^{-1} when ^{18}O is substituted in the bridge, is assigned to the symmetric stretching vibration of the bent V(III)−O−V(III) unit, ν_s(VOV). The magnitude of the isotopic shift of this band (16 cm^{-1}) is consistent with those of the analogous ν_s(FeOFe) and ν_s(MnOMn) stretches at 530 and 558 cm^{-1}, respectively; upon $^{18}O \rightarrow {}^{16}O$ exchange these ν_s modes shift to 513[33a] and 541 cm^{-1}.[24] The first and second overtone vibrations of the symmetric V−O−V stretching mode can also be detected, $2\nu_s$ at 1070 cm^{-1} (Figure 7) and $3\nu_s$ at 1606 cm^{-1} (not shown). The corresponding ν_{as}(FeOFe) and ν_{as}(MnOMn) stretches occur at 754 and 717 cm^{-1}, respectively, as determined from their shifts to 721 and 680 cm^{-1} upon μ-^{18}O substitutions. The

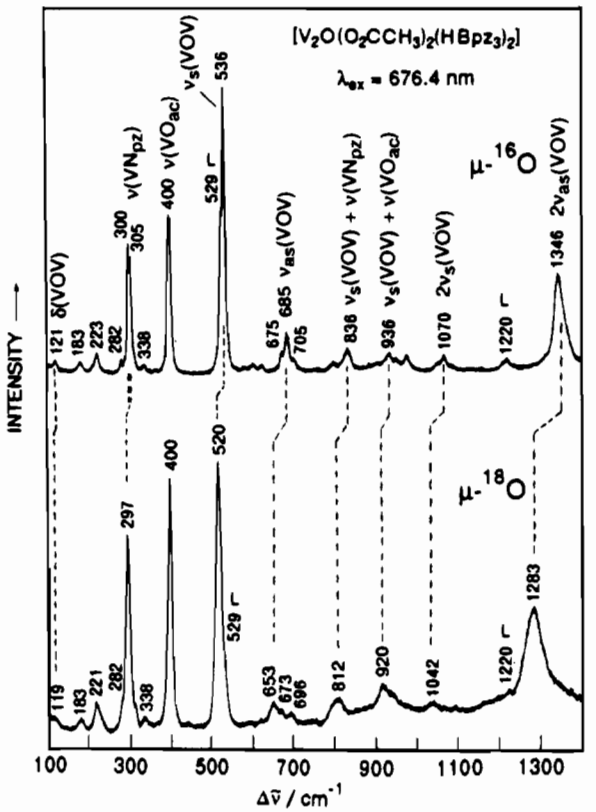

Figure 7. Low-temperature (77 K) resonance Raman spectra of crystalline **I** and its μ-^{18}O isotopomer obtained with 676.4-nm excitation (200 mW) and 5-cm^{-1} slit widths from a KCl pellet attached to a liquid N_2 cell cold finger.[17] "L" marks bands associated with internal modes of $HB(pz)_3^-$ ligands. Subscripts: ac = acetate; pz = pyrazole.

analogous ν_{as}(VOV) could be located at 685 cm^{-1} in the RR spectrum of **I** via its similarly large (32 cm^{-1}) $^{18}O \rightarrow {}^{16}O$ isotopic shift. Additional support for this assignment is provided by a strongly enhanced Raman band at 1346 cm^{-1}, which shifts to 1283 cm^{-1} in the ^{18}O spectrum. Inasmuch as the 1346-cm^{-1} band shows a 63-cm^{-1} ^{18}O-downshift, very close to the twice the frequency shift of the 685 cm^{-1} fundamental (32 × 2 = 64 cm^{-1}), this band must arise from the first overtone of the asymmetric V−O−V stretch, $2\nu_{as}$(VOV). Such an overtone is expected to be highly Raman active from symmetry considerations ($B_2 \times B_2 = A_1$). Similarly, strong $2\nu_{as}$(FeOFe) and $2\nu_{as}$(MnOMn) are observed at 1504 cm^{-1} (1432 cm^{-1}, ^{18}O) and 1432 cm^{-1} (1360 cm^{-1}, ^{18}O), respectively. The assignment of the 536- (ν_s) and 685-cm^{-1} (ν_{as}) Raman peaks is further

(32) Armstrong, W. H.; Spool, A.; Papaefthymiou, G. C.; Frenkel, R. B.; Lippard, S. J. *J. Am. Chem. Soc.* **1984**, *106*, 3653.
(33) (a) Czernuszewicz, R. S.; Sheats, J. E.; Spiro, T. G. *Inorg. Chem.* **1987**, *26*, 2063. (b) Czernuszewicz, R. S.; Dave, B. K.; Rankin, J. G. In *Spectroscopy of Biological Molecules*, Hester, R. E.; Girling, R. B., Eds., Royal Chemical Society: Cambridge, England, 1991; p 285.

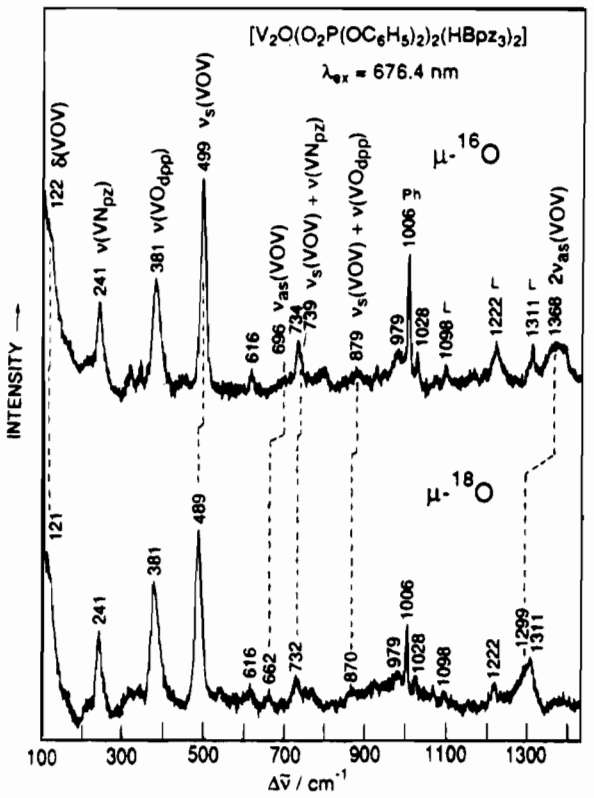

Figure 8. Room-temperature resonance Raman spectra of crystalline **X** and its μ-^{18}O isotopomer obtained with 676.4-nm excitation (100 mW) and 6-cm^{-1} slit widths from a rotating KCl pellet.[16] "L" and "Ph" mark bands associated with internal modes of $HB(pz)_3^-$ ligands and phenyl rings, respectively. Subscripts: pz = pyrazole; dpp = diphenylphosphate.

substantiated by solving the simple secular equations[34] for a bent V−O−V triatomic oscillator. The stretching and stretch-stretch interaction force constants are K_d = 3.31 mdyn/Å and k_{dd} = 1.12 mdyn/Å, respectively. From these force constants we calculate ν_s = 521 cm^{-1} and ν_{as} = 652 cm^{-1} for [^{18}O]-**I**, which are within 1 cm^{-1} of the observed values of 520 (ν_s) and 653 (ν_{as}) cm^{-1}. The other RR bands are assigned to the stretching of terminal V−N(pyrazole) and bridging V−O(acetate) bonds and their combinations bands with ν_s(VOV) as indicated in Figure 7, and an ^{18}O-sensitive peak at 121 cm^{-1} is identified with a predominantly δ(VOV) bending mode.[33a]

The substitution of acetates with diphenylphosphates shifts the symmetric and asymmetric V−O−V stretches in **X** to 499 and 696 cm^{-1}, respectively (Figure 8). The magnitude of the isotopic shift upon labeling the oxo group with ^{18}O changed as well; it decreased for the symmetric stretch, from 16 cm^{-1} (**I**) to 10 cm^{-1} (**X**), but increased for the asymmetric one, from 32 cm^{-1} (**I**) to 34 cm^{-1} (**X**). A characteristically more intense $2\nu_{as}$(VOV) at 1368 cm^{-1} further supports the assignment of the fundamental at 696 cm^{-1}; in [^{18}O]-**X** this band shifts downward by 69 cm^{-1}, as expected for the first overtone (2 × 34 = 68 cm^{-1}). This pattern of vibrational frequencies and isotopic shifts (lower frequency and smaller ^{18}O shift for ν_s but higher frequency and larger ^{18}O shift for ν_{as}) in the phosphate complex is consistent with the larger V−O−V angle found for this complex (Table 4). Using either the valence force constants derived above for **I** or the ^{16}O and ^{18}O vibrational frequencies observed for **X**, a simple triatomic normal mode calculation gives a value of 142° for the V−O−V angle in **X** which agrees well with the crystallographically determined angle of 144°.

(34) Wing, R. M.; Callahan, K. P. *Inorg. Chem.* **1969**, *8*, 871.

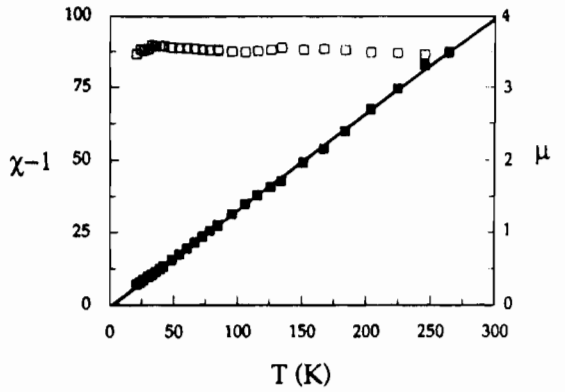

Figure 9. Plot of effective magnetic moment (right, open squares) and molar susceptibility per V_2 dimer (left, filled squares) for **III** as a function of temperature. The line represents the best least-squares fit of the inverse susceptibility to the Curie−Weiss equation.

Finally, although the transitions in the visible region of vanadium μ-oxo dimers have traditionally been ascribed to μ-O→V CT, there has been no definitive proof confirming this assignment. Thus, an excitation profile for the symmetric stretch of the V−O−V core in $[V_2O(O_2CCH_3)_2(HB(pz)_3)_2]$ (**I**) was obtained (data not shown). The Raman intensity of the ν_s(VOV) mode as a function of excitation wavelength traces the UV−visible absorption spectrum of the complex, although the enhancement factors near the red absorption band are much larger. These results prove that the resonance enhancement conferred to the ν_s(VOV) derives from the absorption bands in the visible region and, conversely, substantiates the nature of both absorption bands as due to the μ-O→V(III) CT transitions.

Magnetism. The susceptibilities of all the unprotonated oxo-bridged dimers reported here have been measured at room temperature both in solution and in the solid state. The effective moments all vary between 3.4−3.5 μ_B/V, a value consistent with an S = 2 system for the dimeric unit. This indicates strong ferromagnetic coupling between the two S = 1 V(III) ions in the dimer, as has been previously observed for many other μ-oxo-bridged divanadium(III) complexes with V−O−V bridging angles between 180−130°.[11] Such strongly ferromagnetically coupled systems should have nearly temperature-independent magnetic moments. This was experimentally verified for compound **III** whose temperature-dependent susceptibility was measured from 8−270 K and exhibited Curie−Weiss behavior [μ_{eff} = 3.47(2) μ_B/V, Θ = 0.6(2) K; Figure 9]. We also note, however, a marked degradation in the magnitude of the magnetic moment over time. This can be traced to slow oxidation of the V(III) to V(IV), since freshly prepared samples always have effective moments comparable to those reported here. This is a possible explanation for anomalously low moments of some previously reported V(III) dinuclear systems.[35,36]

In contrast to the above described magnetic behavior, that of the μ-hydroxo-bridged complexes varied markedly with structure. The susceptibility of the protonated propionate complex, **VIIb**, was measured as a function of temperature. It initially increases with decreasing temperature, reaches a maximum at 83 K, and then sharply decreases toward zero with decreasing temperature. This is consistent with an antiferromagnetic interaction between the two spins on the vanadium atoms. The Curie-like tail at the lowest temperature results from a small amount of a paramagnetic impurity (presumably the unprotonated dimer) present in the antiferromagnetic sample. A

(35) Brand, S. G.; Edelstein, N.; Hawkins, C. J.; Shalifmoff, G.; Snow, M. R.; Tiekink, E. R. T. *Inorg. Chem.* **1990**, *29*, 434.
(36) Money, J. K.; Folting, K.; Huffman, J. C.; Christou, G. *Inorg. Chem.* **1987**, *26*, 944.

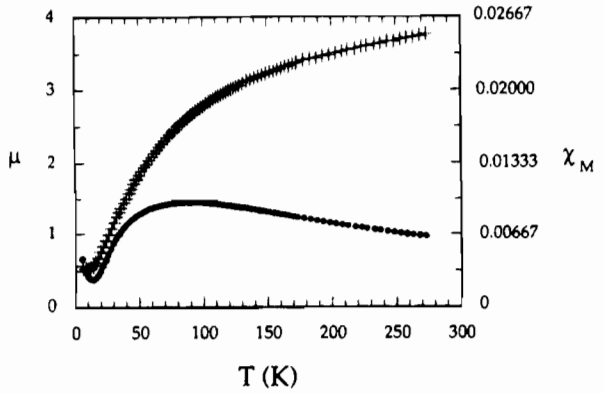

Figure 10. Plot of effective magnetic moment (left, crosses) and molar susceptibility per V_2 dimer (right, filled circles) for **VIIb** as a function of temperature. Solid curve represents the results of a best fit of χT data to an $S = 1$ HDVV model.

nonlinear least-squares fit of the χT vs T data using an $S = 1$ dimer model ($H = 2J\mathbf{S}_1\cdot\mathbf{S}_2$) with impurity ($x$) and TIP corrections yields excellent agreement with the observed data for the parameters $J = -31.3(2)$ cm^{-1}, $g = 2.01(1)$, $x = 0.007(1)$, and TIP = 0.007(1) (Figure 10). The values for J and g also agree well with those reported for the analogous tacn complex by Wieghardt and co-workers.[11] Different behavior is observed, however, for the protonated phosphate derivative, **XI**, where a value of μ_{eff} of 2.96 μ_B/V was measured, the magnitude and temperature independence of which indicates a simple uncoupled $S = 1$ system (data not shown).

Discussion

Structural and magnetic data have been now measured for the series of unsupported μ-oxo[37] and supported μ-oxo, bis(μ-carboxylato)[12] M(III) dimers (M = Ti–Fe) and the μ-hydroxo analogs of the latter (M = V,[11] Cr,[38] and Fe[39]). A simple MO scheme, first derived by Dunitz and Orgel for unsupported dimers,[40] can be used to rationalize many of the structural and magnetic properties of these systems. The mononuclear fragment of the dimer, an irregular octahedron compressed along the V–O_{oxo} axis, provides a t_{2g} orbital manifold, split into a singlet ($d_{x^2-y^2}$) and a doublet (d_{xz}, d_{yz}), and an e_g manifold, split into two orbital singlets (d_{xy} low, d_{z^2} high) as shown at the far left in Figure 11. Symmetric (s) and antisymmetric (as) combinations of these mononuclear fragment orbitals will produce the MO's of the unsupported dimer into which the metal d-electrons will be placed (Figure 11). Thus in a Ti(III) dimer (d^1) the pair of metal electrons will go into the almost degenerate $d_{x^2-y^2}$ MO manifold resulting in a weak exchange coupling.[37] On the other hand, the additional pair of electrons in a V(III) dimer (d^2) will go spin parallel into the 2-fold degenerate (d_{xz}, d_{yz})$_{as}$ manifold to produce strong ferromagnetic (FM) coupling.[41] Since the (d_{xz}, d_{yz})$_s$ manifold is significantly higher in energy, the third pair of electrons in a Cr(III) dimer (d^3) will fill the (d_{xz}, d_{yz})$_{as}$ level to give the observed strong antiferromagnetic (AFM) coupling.[42]

Addition of two cobridging ligands to the linear unsupported μ-oxo dimers leads to the bent M–O–M backbone characteristic

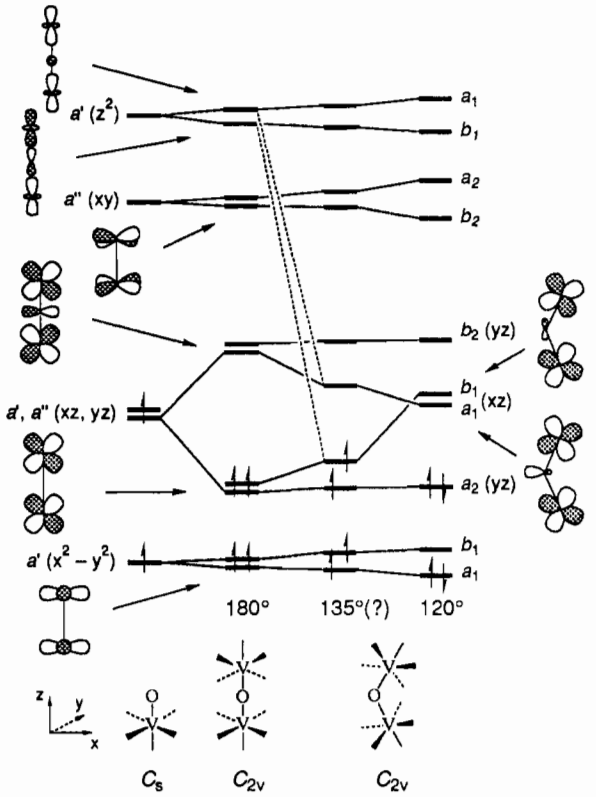

Figure 11. Qualitative molecular orbital diagram for linear and bent oxo-bridged M(III) dimers.

of the supported μ-oxo M(III) dimers. Since the loss of metal–oxygen π-bonding will resist this bending, counterbalancing forces must exist. Obviously, accommodation of the cobridging ligands is the major force in forming the bent dimers, but a change in the hybridization of the bridging oxygen from sp to sp^2 also appears to stabilize the system. Except in the V(III) system, M–O–M angles are all close to 120°, the ideal for an sp^2 oxygen, with almost no change in this angle upon protonation, i.e., when sp^2 hybridization is clearly present. In contrast, the supported μ-oxo V(III) dimer has a significantly larger M–O–M angle (~133°) that decreases dramatically upon protonation (to ~123°). This situation prevails in the bis(μ-phosphato) systems where protonation again yields an approximate 10° decrease in bridge angle in spite of the larger angle imposed by the "bite" of the cobridging phosphates. It appears, then, that the μ-oxo V(III) dimers are driven toward an absolute conformational energy minimum at $\angle(M\text{–O–}M) \approx 180°$ rather than toward the local minimum $\angle(M\text{–O–}M) \approx 120°$ as the other μ-oxo and all μ-hydroxo dimers are. Does this structural anomaly bear any relation to the unusually large FM coupling in the supported μ-oxo V(III) dimers?

Consideration of the MO scheme for the bent M–O–M dimer systems (Figure 11, right) provides some insight. Upon bending, the orbital degeneracies inherent in the linear systems are lost and result in changes in magnetic properties. Increased overlap between $d_{x^2-y^2}$ orbitals with bending will, for example, lift the near-degeneracy in the lowest energy MO manifold leading to spin pairing and strong AFM coupling as in the bent Ti(III) dimers.[43] In the (d_{xz}, d_{yz}) MO manifold, the energies of the (d_{yz})$_s$ and (d_{yz})$_{as}$ MO's will be relatively constant through the range of bending, but the (d_{xz})$_{as}$ MO will become more antibonding and the (d_{xz})$_s$ MO less antibonding in energy as $\angle(M\text{–O–}M)$ decreases with the two becoming degenerate at

(37) Jeske, P.; Wieghardt, K.; Nuber, B. *Inorg. Chem.* **1994**, *33*, 47 and references therein.
(38) Turowski, P. N.; Bino, A.; Lippard, S. J. *Angew. Chem. Int. Ed. Engl.* **1990**, *29*, 811.
(39) Armstrong, W. H.; Lippard, S. J. *J. Am. Chem. Soc.* **1984**, *106*, 4632.
(40) Dunitz, J. D.; Orgel, L. E. *J. Chem. Soc.* **1953**, 2594.
(41) Knopp, P.; Wieghardt, K.; Nuber, B.; Weiss, J.; Sheldrick, W. S. *Inorg. Chem.* **1990**, *29*, 363.
(42) Holwerda, R. A.; Tekut, T. F.; Gafford, B. G.; Zhang, J. H.; O'Connor, C. J. *J. Chem. Soc. Dalton Trans.* **1991**, 1051.
(43) Bodner, A.; Drueke, S.; Wieghardt, K.; Nuber, B.; Weiss, J. *Angew. Chem. Int. Ed. Engl.* **1990**, *29*, 68.

Table 8. Magnetostructural Data for Selected (μ-Oxo/Hydroxo) V(III) Dimers

compound	V−O−V angle, deg	magnetic coupling
μ-oxo[a]	180	ferromagnetic
μ-oxo[b]	174	ferromagnetic
μ-oxo[c]	154	ferromagnetic
(μ-oxo)bis(μ-phosphato)[d]	144	ferromagnetic
(μ-oxo)bis(μ-acetato)[d]	133	ferromagnetic
(μ-hydroxo)bis(μ-phosphato)[d]	133	uncoupled
(μ-hydroxo)bis(μ-acetato)[d]	123	antiferromagnetic

[a] $[V_2O(tacn)(acac)]\cdot 2H_2O$.[41] [b] $[V_2O(bpy)_2Cl_2]\cdot 6H_2O$.[35] A temperature independent effective moment is reported (3.18 μ_B/V) that is significantly above the isolated spin value. [c] $[V_2O(l\text{-his})_2]\cdot 2H_2O$.[45] A room temperature moment of 3.20 μ_B/V has been measured for the solid compound (Bond, M. R., unpublished work). [d] This work.

~120°. The greater dispersion in energy of the (d_{xz}, d_{yz}) MO's in the bent systems places excited electronic states closer to the ground state. Hence, AFM coupling in the d^3 Cr(III) dimer should be substantially less than in the linear analog, as found experimentally.[25a] The situation for the bent V(III) systems is, however, less clear. Upon bending, the $(d_{yz})_{as}$ MO is left the lowest energy orbital of the (d_{xz}, d_{yz}) manifold. To a first approximation, the lowest orbital energy of a d^2 V(III) dimer will be attained with metal electrons spin-paired in this MO. This, however, ignores the large spin-pairing energy that would accompany this electronic configuration. While an experimental determination of this energy has not been made, it would appear to be quite large from the fact that ferromagnetic spin alignment prevails even at room temperature in the linear systems. Indeed, a recent *ab initio* calculation has placed the energy of the singlet state over 2000 cm^{-1} above the FM ground state in a model, linear V−O−V dimer.[44] One should expect, then, that the FM coupling of the linear dimer should persist as ∠(V−O−V) decreases until the gain in orbital energy obtained through spin-pairing exceeds the spin-pairing energy itself. At this point the exchange coupling should switch from FM to AFM. Yet the experimental observations are consistent with FM coupling throughout the ∠(V−O−V) from 180 to 135° as has been summarized for representative compounds in Table 8. The observed bridge angle strain toward the linear value in the V(III) systems is also consistent with this model since orbital energy is minimized when the bridge angle is maximized within the limits imposed by the cobridging ligands.

Protonation of the dinuclear bis(μ-carboxylato)-supported complex produces a V−O−V angle (123.5°) consistent with the imposition of sp^2 hybridization at the bridging oxygen. Accompanying this structural change is the crossover from strong FM to moderate AFM coupling as shown in Table 8. In discussing the origin of the strong FM coupling in the unprotonated dimers, we postulated that the exchange coupling could change from FM to AFM once the bridge angle reached a value beyond which the gain in orbital energy exceeds the cost in spin-pairing energy. In fact, in the (μ-hydroxo)bis(μ-phosphato) complex, where the bridge angle is substantially larger, the coupling is indeed more ferromagnetic than in the corresponding carboxylates. It could be argued from these results that one observes the same trend here as postulated for the unprotonated species, i.e. AFM coupling at low bridge angle crossing over to FM coupling at high angle, but with the overall magnitude of the coupling attenuated as a result of V−O_{oxo} bond lengthening. However, the structural changes wrought by protonation are sufficiently large that simple comparison of electronic and magnetic properties between the two classes is a perilous endeavor. Nevertheless, the structural and magnetic properties of both protonated and unprotonated systems illustrate the importance of the bridge geometry in analyzing the physical and chemical behavior of this family of dinuclear complexes.

A clear correlation between structure, i.e. V−O−V bridging angle, and resonance Raman or UV−visible spectroscopic properties is also evident in the data presented here. For example, Figure 5 shows the optical spectral data for (μ-oxo)-bis(μ-acetato or μ-phosphato), and μ-oxo−V(III)−tris(pyrazolyl)borate complexes whose V−O−V angles vary from 133 to 180°. As can be seen, the highest energy band (band 3) decreases rapidly in intensity as the angle opens up while the mid-energy (band 2) increases concomitantly. The low energy (band 1) both decreases in intensity and shifts to higher energy with increasing angle. A plot of the ratio of $I(\lambda_2)/I(\lambda_1)$ vs angle is linear, at least for this narrow range of very similar compounds. Similar complexes with aromatic nitrogen ligands *trans* to the oxo group, such as those of phenanthroline and bipyridine, fit less well to the line but are still reasonably correlated, whereas complexes without such aromatic nitrogen donors do not correlate well at all. The differences in geometry and electronic structures of the V−O−V bridge in (μ-oxo)-divanadium(III) complexes are also reflected in the characteristic frequencies and intensities of vanadium-oxo stretching resonance Raman bands. Similar to the Fe(III) and Mn(III) (μ-oxo) dimers, the unique feature of the bent V(III)−O−V(III) unit is a very intense symmetric stretch, ν_s(VOV) at ~500 cm^{-1}, and a weak asymmetric stretch, ν_{as}(VOV) at ~700 cm^{-1}. The ν_s(VOV) and ν_{as}(VOV) occur at 536 and 685 cm^{-1}, respectively, in the acetate complex **I** (Figure 7), but at 499 (ν_s) and 699 (ν_{as}) cm^{-1} in the phosphate complex **X** (Figure 8). These frequencies conform to the values expected for the V−O−V angles seen in the crystal structures of **I** and **X**, ~134 and ~144° (Table 4); the ν_s and ν_{as} are expected to shift downward and upward, respectively, upon widening of the μ-oxo bridge angle. The V(III) μ-oxo dimers are, however, unique in that the symmetric stretch is *not* observed when the V−O−V angle exceeds the value of 155°. As recently demonstrated by us[22,45] and others,[9] the characteristic features of such complexes are only the moderately enhanced asymmetric V−O−V stretch and a very intense first overtone of the asymmetric fundamental, $2\nu_{as}$(VOV). In order to provide answers for these puzzling behavior, more systematic studies of the effects of V−O−V angle on the bridge vibrational frequencies and Raman intensities, including detailed excitation profile measurements, are currently in progress.

Concluding Remarks

The oxo-bridged dinuclear vanadium(III) complexes stand out from among the family of oxo-bridged dimetal(III) complexes because of their exceptional physical properties. By preparing and characterizing a series of bis(μ-carboxylato) and bis(μ-phosphato), μ-oxo/μ-hydroxo species, we have been able to study the effects on these properties caused by changes in the bridging V−O−V angle and in the coordination number of the bridging oxygen. The structural and magnetic data gathered for these complexes have contributed to our understanding of their electronic structure and conformational properties. Our magnetic results indicate that strong *ferromagnetic* coupling persists through the V−O−V angle range 180−130° in the μ-oxo compounds, but that the μ-hydroxo compounds become less *antiferromagnetic* as the V−O(H)−V angle increases from

(44) Fink, K.; Fink, R.; Staemmler, V. *Inorg. Chem.* **1994**, *33*, 6219.

(45) Czernuszewicz, R. S.; Yan, Q.; Bond, M. R.; Carrano, C. J. *Inorg. Chem.* **1994**, *33*, 6116.

120°. Spectroscopic data have proven more sensitive to changes in the bridge angle, the resonance Raman lines showing characteristic frequency shifts and the visible spectra showing characteristic intensity variations that correlate well with the observed structural changes. We hope that these results will be useful in the study of oxo-bridged vanadium species in biological systems.

Acknowledgment. This work is partially supported by Robert A. Welch Foundation Grants AI-1157 (C.J.C.) and E-1184 (R.S.C.) and by Grant GM-48370 from the National Institutes of General Medical Sciences, NIH (R.S.C). C.J.C. also wishes to acknowledge the Texas Advanced Research Program Grant 3615-002 and the NIH AREA Grant GM4767601 for additional support. The NSF-ILI Programthrough Grant USE-9151286 is acknowledged for support of the X-ray diffraction facilities at Southwest Texas State University.

Supporting Information Available: Text and a table giving full details of the crystal structure determinations and tables of crystallographic conditions and parameters, atomic coordinates and equivalent isotropic thermal parameters, bond lengths and angles, anisotropic displacement parameters, and H-atom coordinates and isotropic thermal parameters for compounds **I**, **VI**, **VIIa**, **X**, and **XI** (39 pages). Supplementary material for compounds **III** and **VIIb** has been deposited with a preceding communication (see ref 13). This material is contained in many libraries on microfiche, immediately follows this article in the microfilm version of this journal, and can be ordered from the ACS; see any current masthead page for ordering information.

IC950795O